Transition metals in photovoltaic-grade ingot-cast multicrystalline silicon: Assessing the role of impurities in silicon nitride crucible lining material ☆

T. Buonassisi[a], A.A. Istratov[a],[*], M.D. Pickett[a], J.-P. Rakotoniaina[b], O. Breitenstein[b], M.A. Marcus[c], S.M. Heald[d], E.R. Weber[a]

[a]*Materials Science Division, Department of Materials Science and Engineering, Lawrence Berkeley National Laboratory, University of California, Berkeley, Building 62-109 (MS 62R0203), 1 Cyclotron Road, Berkeley, CA 94720, USA*
[b]*Max Planck Institute of Microstructure Physics, Halle, Germany*
[c]*Advanced Light Source, Lawrence Berkeley National Laboratory, Berkeley, CA 94720, USA*
[d]*Advanced Photon Source, Argonne National Laboratory, Argonne, IL 60439, USA*

Available online 4 January 2006

Abstract

We assess the contamination potential of crucibles used during directionally solidified multicrystalline silicon (mc-Si) ingot casting for cost-effective solar cell wafer production. Highly sensitive, synchrotron-based analytical microprobe techniques were used to study the distributions, sizes, elemental natures and chemical states of impurity-rich particles in α-Si_3N_4 powder representative of what is used to coat the inside of mc-Si ingot-casting crucibles, as well as the as-grown cast mc-Si material. Correlations between the elemental species, chemical states, particle sizes, relative concentrations and locations of impurities (e.g. Fe, Ti, Ca, Zn, Ni, Cu, N, C) concomitant in α-Si_3N_4 and as-grown mc-Si lead us to conclude that α-Si_3N_4 could be a significant source of contaminants during the ingot-casting mc-Si growth process.
© 2005 Elsevier B.V. All rights reserved.

1. Introduction

Recent neutron activation analysis (NAA) studies revealed metal concentrations in ingot-cast multicrystalline silicon (mc-Si) materials as high as 10^{13}–$10^{16}\,cm^{-3}$ (i.e., in the ppb to ppm range) [1–3]. Subsequent studies [4,5] indicated that the majority of metals are present either in (a) metal silicide nanoprecipitates typically $<100\,nm$ in diameter, composed of medium- or fast-diffusing metal species, and present in high spatial densities (especially along structural defects), or (b) larger particles up to several microns in size, often in an oxidized chemical state and/or containing multiple slowly diffusing impurity species, present in low spatial densities. A model was developed [5] to explain the presence of both types of particle in mc-Si—the metal silicide nanoprecipitates form from supersaturated metal atoms dissolved within the melt or the crystal, while the micron-sized particles are likely to be inclusions of foreign particles that enter the melt and are incorporated by the advancing solidification front. Understanding the sources and mechanisms of metal contamination is a vital first step to reduce metal contamination levels in mc-Si solar cells.

In this manuscript, we assess the contamination potential of crucibles used during directionally solidified mc-Si ingot casting (i.e. the technology that currently produces

---

over 50% of solar cells worldwide). This source of contamination is important for the casting technology because of the prolonged contact (several tens of hours) between the crucible (usually a fused silica or graphite crucible lined with a silicon nitride coating) and the silicon melt/crystal during ingot production. If impurities are contained within any of the crucible parts, then contamination of the melt or of the cooling ingot may occur, as suggested by previous studies (e.g., Refs. [6–11]).

2. Materials and methods

Two types of material were analyzed in this study: (a) α-Si_3N_4 powder, and (b) as-grown mc-Si wafers produced from cast ingots.

Samples of α-Si_3N_4 powder were obtained from commercial chemical suppliers (Alfa Aesar and Cerac) and from one of our industrial collaborators; the latter material is representative of what is used in industry to coat the insides of mc-Si ingot-casting crucibles. Four types of commercial α-Si_3N_4 powders were analyzed, with vendor-specified purities ranging from 95% to 99.9%, in addition to the industrial sample. Each type of powder was poured into a small satchel of 5 µm-thick clean polymer and then attached to a sample stage. A background scan on an empty polymer satchel revealed no impurity particles above the detection limits, ensuring that the impurity particles detected by µ-XRF indeed originated from the powder samples themselves.

As-grown ingot-cast mc-Si wafers were extracted from near the bottom, middle, top and edges of several ingots grown by different manufacturers. All samples were lightly etched to remove surface contamination before being measured by highly sensitive synchrotron-based techniques. One particular sample that contained a high density of Si_3N_4 and SiC microdefects was cut vertically from the upper 2 cm of a directionally solidified ingot, as described in Ref. [12]. The wafer was then polished down to ~0.25 µm mean surface roughness for study by infrared transmission microscopy. During the final stage of the polishing process, it was noticed that some microdefects were revealed at the surface of the wafer and could be observed by an optical microscope. These "partially unburied" microdefects were selected for microanalysis by synchrotron-based techniques, after a light etching to remove surface contaminants.

Synchrotron-based X-ray fluorescence microscopy (µ-XRF) was used to map distributions of impurity-rich particles, to identify their elemental compositions, and to determine their sizes. Once impurity-rich particles were located by µ-XRF, their chemical states (e.g., oxide vs. silicide) were identified by the X-ray absorption microspectroscopy (µ-XAS) technique. Details of these experimental techniques can be found in Refs. [4,5,13,23].

To perform µ-XRF/XAS measurements, we used beamline 10.3.2 [14] of the Advanced Light Source at Lawrence Berkeley National Laboratory, and beamline 20-ID-B [15]

at the Advanced Photon Source of Argonne National Laboratory.

Infrared transmission microscopy (IRTM, performed at MPI Halle) was used to locate Si_3N_4 and SiC microdefects and to observe their structures, which were then correlated to transmission electron microscopy measurements on similar samples to determine their chemical compositions. Energy dispersive X-ray microanalysis (EDX, performed at MPI Halle) confirmed the presence of C and N at these microdefects.

3. Results

3.1. α-Si_3N_4 crucible lining material

The total impurity contents of α-Si_3N_4 powders from commercial suppliers were obtained by inductively coupled plasma optical emission spectroscopy (ICP-OES, performed by the vendors). Fig. 1a shows the results of these analyses, i.e., the most common impurities in α-Si_3N_4. Interestingly, most major impurities, as well as their concentrations, are very similar to those reported [16,17] in α-Si_3N_4 powders studied during the 1970s.

For comparison, Fig. 1b shows impurity content of ingot-cast mc-Si as determined by NAA. Not all elements detected by ICP-OES and plotted in Fig. 1a could be detected in mc-Si by NAA, because NAA is not equally sensitive to all elements [18], and vice versa; hence, the lack of bars in Fig. 1(a) or (b) corresponding to certain elements does not imply that these elements were not present, but
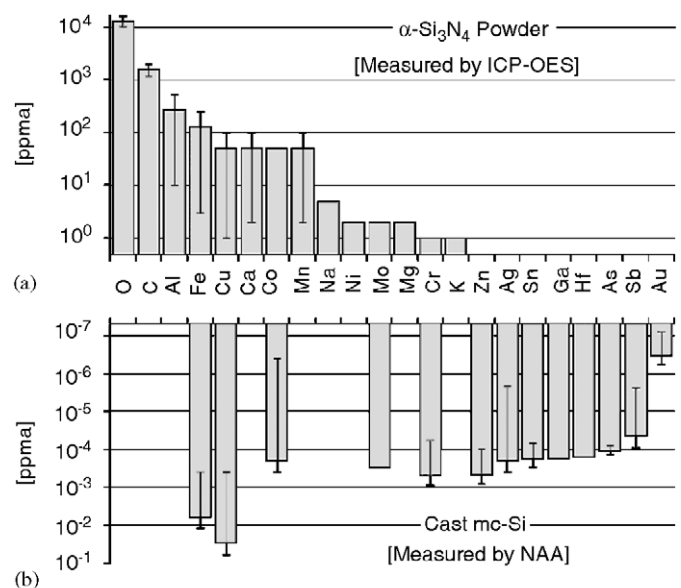

Fig. 1. (a) Vendor-specified impurity contents of four different commercially available α-Si_3N_4 powders with purities between 95% and 99.9%. The range of variation, which depends on the purity of the powder, is shown by the error bars. (b) Impurity content of different directionally solidified ingot-grown mc-Si materials determined by NAA [1–3]. The error bars show the range of values obtained on different samples.

rather means that they could not be detected by a particular analytical technique. The μ-XRF technique, used in our experiments to map distributions of impurities, can easily detect elements such as Fe and Ca, which are some of the most abundant metal impurities, but cannot readily detect lighter elements such as O, N, C and Al, since their fluorescence energies are below 1.5 keV and are strongly absorbed by silicon and air.

Fig. 2 shows a μ-XRF map of Fe and Ca distributions in an α-Si$_3$N$_4$ powder provided by our industrial collaborator, and typical of what is used in industry to coat the ingot-casting crucibles. Similar distributions were observed in the powders purchased from commercial vendors. In such powders, iron can be found both distributed homogeneously as well as concentrated in discrete small and large particles. The homogeneously distributed background iron concentration is most readily detectable in lower-purity α-Si$_3$N$_4$, and is determined by μ-XAS to be in the FeSi$_2$ chemical state. In addition, discrete Fe-rich particles can be observed in all α-Si$_3$N$_4$ materials. The sizes and abundances

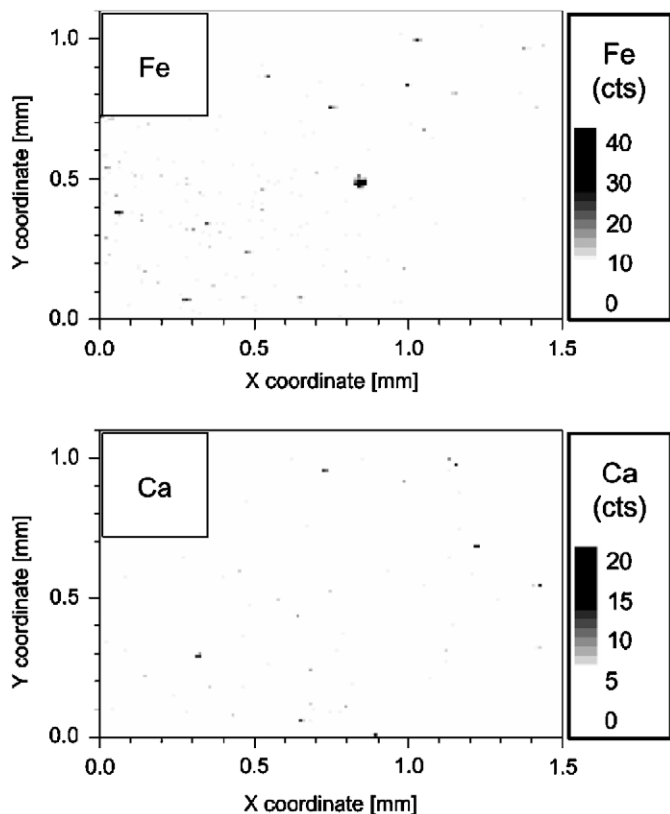of these particles decrease with increasing powder purity; the industrial sample demonstrated particle sizes and abundances comparable to the higher-purity commercial samples. These particles exist in two varieties—larger particles of a chemical state most similar to Fe$_2$O$_3$ (Fig. 3a), and smaller particles of Fe + Cr + Ni (reminiscent of stainless steel, Fig. 4) with iron in an Fe^0 charge state (such as in iron silicide, metallic iron, iron carbide, etc.) (Fig. 3b). Other less-frequently observed impurity-rich particles contain Cu metal, Zn, Ti, Cr, Ni, Co or Ca. All α-Si$_3$N$_4$ powders analyzed in this study exhibit at least two of these types of particle, in addition to the more abundant Fe-rich particles.

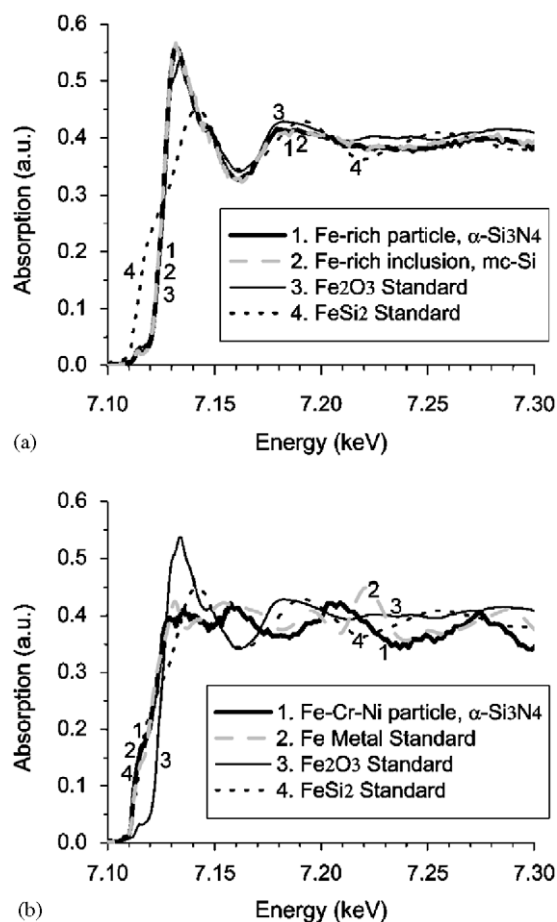Fig. 2. μ-XRF map of α-Si$_3$N$_4$ powder (representative of what is used in industry to coat casting crucibles) reveals the spatial distribution of iron- and calcium-rich particles. Both large and small iron-rich particles are observed. Large Fe-rich particles (such as the one at X = 0.7 mm, Y = 0.5 mm) contain only iron in a chemical state most similar to Fe$_2$O$_3$ (Fig. 3a). The smaller particles consist of Fe + Ni + Cr (Fig. 4), with iron in a Fe^0 charge state, i.e. most similar to metallic Fe (Fig. 3b). Background Fe, detectable in some lower-purity α-Si$_3$N$_4$ powders, is determined to be FeSi$_2$. More isolated particles containing Cu metal, Zn, Ti, Cr, Ni and Co were also observed.

Fig. 3. μ-XAS spectra of two types of Fe-rich particle in α-Si$_3$N$_4$ material. The particle in (a) contains a large amount of iron (Fig. 2), and the chemical state is most similar to iron oxide (Fe$_2$O$_3$). The particle in (b) consists of Cr, Ni and Fe (Figs. 2 and 4), and the near-edge features match most closely with those of iron in the Fe^0 charge state (e.g. Fe metal, Fe silicide), although the extended X-ray absorption fine spectrum does not match perfectly with any of the standards. Note that the μ-XAS of the oxidized iron particle found in α-Si$_3$N$_4$ and that of an oxidized iron inclusion detected in ingot-cast mc-Si material match nearly perfectly, indicating that both the charge state and local crystallographic environment are nearly identical, and providing strong evidence that metal-rich particles in the α-Si$_3$N$_4$ crucible lining material can enter the melt during growth.
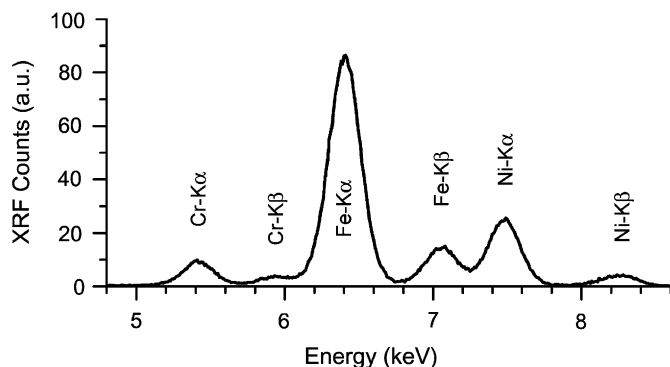
Fig. 4. Typical μ-XRF point spectrum of the smaller Fe-rich particles in Fig. 2. Iron, chromium and nickel are present in proportions suggestive of stainless steel. The μ-XAS spectrum for this particle appears in Fig. 3b.

Fig. 5. (a) IRTM image of a β-Si$_3$N$_4$ rod encircled by SiC clusters, found in the upper part of a cast mc-Si ingot; (b–d) μ-XRF maps of the same region. Homogeneously distributed Ca and FeSi$_2$ are present at the β-Si$_3$N$_4$ rod. Particles of FeSi$_2$ and Cu$_3$Si are also present at the SiC clusters. All of these impurities are also present in α-Si$_3$N$_4$ powder in high concentrations (Figs. 1 and 2).

3.2. Metals in ingot-cast mc-Si

The spatial distributions and chemical states of metal-rich particles in ingot-cast mc-Si turned out to be very similar to those in the silicon nitride coating. In ingot-cast mc-Si, three types of impurity-rich particle are observed by our experimental techniques: (a) metal silicide nanoprecipitates, typically 30–60 nm in diameter, most often found along structural defects (especially grain boundaries), (b) metal-rich inclusions, often measuring up to a few tens of microns in diameter, and (c) extended microdefects (e.g., silicon carbide or nitride) measuring up to several tens or hundred of microns in diameter. Note that the experimental techniques used in this study are insensitive to most metal point defects, such as individual interstitial or substitutional metal atoms.

The metal silicide nanoprecipitates detected in ingot-cast mc-Si are usually found at structural defects (e.g., grain boundaries) and typically contain Ni, Fe, Cu and/or Co, incidentally the 3d transition metal species with highest solubilities and diffusivities in silicon. Further details on structure and properties of metal particles in silicon can be found in our recent publications [4,5,19]. A much higher concentration of these precipitates is observed towards the bottom, top and edges of the ingot. The total amount of metals contained in these precipitates is estimated by μ-XRF to reach values as high as 3×10^{14} cm^{-3} [5] or higher. On the other hand, in the middle of the ingot, such precipitates are rarely observed above the current μ-XRF detection limits.

Micron-sized particles in mc-Si are often composed of oxidized Fe or Ti (an example of such particle is shown in Ref. [5]). In addition, particles containing Ca, Zn, Mn, Mo and/or Cr, with traces of fast diffusers were also observed. The abundance of slowly diffusing elements, combined with their frequently oxidized chemical state lead us to conclude that these particles are inclusions and not precipitates [4,5]. The spatial density of these particles is orders of magnitude lower than metal silicide nanoprecipitates. However, each in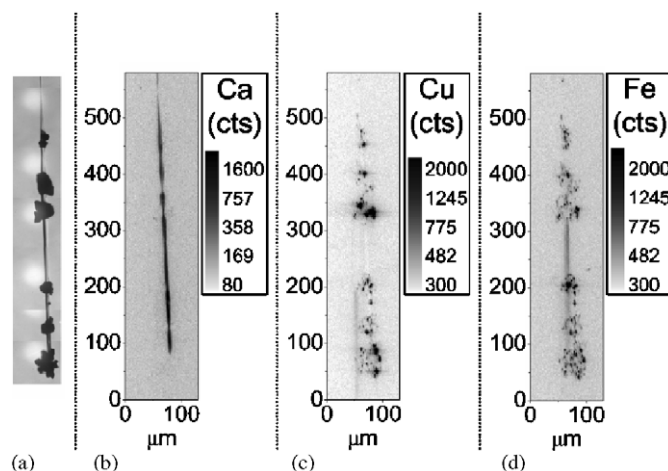clusion particle contains a far greater number of metal atoms than a metal silicide nanopreciptiate. Consequently, these particles were found to account for local metal contents as high as 2.3×10^{16} cm^{-3} [5] in regions of the ingot where they are most prevalent (top, bottom and edges).

Metals are also found at Si$_3$N$_4$ and SiC microdefects towards the top of the ingot. These microdefects are specific for ingot-cast mc-Si; the significance of finding these microdefects is discussed below. An IRTM image (Fig. 5a) of one collection of microdefects reveals a β-Si$_3$N$_4$ rod surrounded by several β-SiC clusters. FeSi$_2$ and Ca (chemical state not determined) are found rather homogeneously distributed within the β-Si$_3$N$_4$ rod (Figs. 5b,d), while FeSi$_2$ and Cu$_3$Si particles are observed within the SiC clusters surrounding the Si$_3$N$_4$ rods (Figs. 5(c) and (d)).

4. Discussion and conclusions

The results presented in this study strongly indicate that the silicon nitride coating could contaminate cast mc-Si ingots with an assortment of metallic and non-metallic impurities during crystal growth. Firstly, the *relative concentrations of elemental impurity species* in α-Si$_3$N$_4$ are similar to those impurities found in ingot-cast mc-Si, as shown in Fig. 1. It must be noted that the bulk impurity concentrations in the nitride coating and ingot-cast mc-Si wafers were measured using different experimental techniques, each sensitive to a different set of elements (e.g., NAA is not well-suited to detect low-Z elements such as carbon and nitrogen, but it has better sensitivity than ICP-OES to some transition metals). Secondly, the *chemical states* of certain impurity-rich particles in α-Si$_3$N$_4$ and inclusions in ingot-cast mc-Si are practically identical, as shown in the overlapping μ-XAS spectra in Fig. 3a. Thirdly, the *distribution* of impurities in ingot-cast mc-Si

ingots suggests an external contamination source in contact with the melt and crystal, given the predominance of precipitates and inclusions near the side edges of ingots. Fourthly, the observation of *silicon nitride and silicon carbide microdefects* in the upper regions of the ingot reflects high concentrations of carbon and nitrogen impurities in the melt. (The precise formation mechanisms of these microdefects is complex and the subject of separate discussions [7,12,20], but it is generally believed that dissolved nitrogen and carbon become supersaturated in the melt during the latter stages of ingot growth, leading to the formation of these microdefects). During directionally solidified cast mc-Si ingot growth, nitride and carbide particles likely decompose from the crucible lining material in contact with the melt. This is consistent with the observation that mc-Si materials not grown in Si_3N_4-coated crucibles seldom exhibit silicon nitride and silicon carbide microdefects, with the exception of silicon carbide microdefects observed in mc-Si materials grown using graphite crucible parts [21] or growth substrates [22]. Upon decomposition of the silicon nitride crucible lining material in contact with the melt, other impurity atoms or particles associated with the nitride can also enter into the melt. This hypothesis is strongly supported by the concomitant presence of N, C, Fe, Ca and Cu at these microdefects (Fig. 5) and within α-Si_3N_4 powders (Figs. 1, 2).

These data suggest two possible mechanisms of incorporating impurities from the crucible lining material coating into mc-Si:

(1) Impurity atoms and impurity-rich particles in the α-Si_3N_4 may dissolve into the silicon melt or warm crystal and form metal point defects, precipitates and/or microdefects. This mechanism likely dominates for small particles (e.g. Fe + Cr + Ni-rich particles), particles with low melting temperatures and impurities distributed atomically or in very small clusters (e.g. background $FeSi_2$ in lower-purity α-Si_3N_4).

(2) Impurity-rich particles in the α-Si_3N_4 may be wholly incorporated into the melt as second-phase particles. If these particles exist for only a short time in the melt, and/or if the melt is already saturated with the given impurity species, then these second-phase particles can be incorporated into the advancing solidification front as inclusions. This is likely to be the case for the relatively large (diameter $\geqslant 1\,\mu m$) oxide-like iron particles occasionally observed in α-Si_3N_4 and near the edges, top, and bottom of mc-Si ingots. It is also possible that certain microdefects are formed this way [7,12,20].

The concentration of impurities in the melt dissolving from the α-Si_3N_4 coating depends on the total thickness of α-Si_3N_4 that dissolves during crystal growth, the elements that may be added during the coating process as sintering aid, as well as on the surface area to volume ratio of the crucible. Effective means of reducing the impact of this contamination source on ingot-cast mc-Si might include reducing the impurity content in α-Si_3N_4, improving the structural quality of Si_3N_4 to minimize its decomposition during growth and reducing the surface area to volume ratio of the crucible (e.g. increasing the crucible size).

Acknowledgments

References

[1] A.A. Istratov, T. Buonassisi, R.J. McDonald, A.R. Smith, R. Schindler, J.A. Rand, J.P. Kalejs, E.R. Weber, J. Appl. Phys. 94 (2003) 6552.

[2] D. Macdonald, A. Cuevas, A. Kinomura, Y. Nakano, L.J. Geerligs, J. Appl. Phys. 97 (2005) 33523.

[3] D. Macdonald, A. Cuevas, A. Kinomura, Y. Nakano, in: 29th Photovoltaic Specialists Conference, IEEE, New Orleans, LA, 2002, p. 285.

[4] T. Buonassisi, M.A. Marcus, A.A. Istratov, M. Heuer, T.F. Ciszek, B. Lai, C. Zhonghou, E.R. Weber, J. Appl. Phys. 97 (2005) 63503.

[5] T. Buonassisi, A.A. Istratov, M. Heuer, M.A. Marcus, R. Jonczyk, J. Isenberg, B. Lai, C. Zhonghou, S. Heald, W. Warta, R. Schindler, G. Willeke, E.R. Weber, J. Appl. Phys. 97 (2005) 74901.

[6] S. Binetti, M. Acciarri, C. Savigni, A. Brianza, S. Pizzini, A. Musinu, Mater. Sci. Eng. B 36 (1996) 68.

[7] A.K. Soiland, E.J. Ovrelid, T.A. Engh, O. Lohne, J.K. Tuset, O. Gjerstad, Mater. Sci. Semicond. Process. 7 (2004) 39.

[8] O. Breitenstein, J.P. Rakotoniaina, M.H.A. Rifai, M. Werner, Progr. Photovoltaics: Res. Appl. 12 (2004) 529.

[9] M. Ghosh, D. Yang, A. Lawerenz, S. Riedel, H.J. Möller, in: 14th European Photovoltaic Solar Energy Conference and Exhibition, Barcelona, Spain, 1997, p. 724.

[10] C. Ballif, S. Peters, C. Borchert, C. Hässler, J. Isenberg, R. Schindler, W. Warta, G. Willeke, in: 17th European Photovoltaics Specialists Conference, Munich, Germany, 2001, p. 1818.

[11] M. Rinio, C. Ballif, T. Buonassisi, C. Borchert, in: 19th European Photovoltaic Solar Energy Conference, Paris, France, 2004, p. 762.

[12] J.P. Rakotoniaina, O. Breitenstein, M. Werner, M. Hejjo Al-Rifai, T. Buonassisi, M.D. Pickett, M. Ghosh, A. Müller, N. Le Quang, in: Proceedings of the 20th European Photovoltaic Specialists Conference and Exhibition, Barcelona, Spain, 2005, pp. 773–776.

[13] S.A. McHugo, A.C. Thompson, C. Flink, E.R. Weber, G. Lamble, B. Gunion, A. MacDowell, R. Celestre, H.A. Padmore, Z. Hussain, J. Crystal Growth 210 (2000) 395.

[14] M.A. Marcus, A.A. MacDowell, R. Celestre, A. Manceau, T. Miller, H.A. Padmore, R.E. Sublett, J. Synchrotron Radiat. 11 (2004) 239.

[15] S. Heald, E. Stern, D. Brewe, R. Gordon, D. Crozier, J. Detong, J. Cross, J. Synchrotron Radiat. 8 (2001) 342.

[16] J.L. Iskoe, F.F. Lange, E.S. Diaz, J. Mater. Sci. 11 (1976) 908.

[17] D.P. Elias, M.W. Lindley, J. Mater. Sci. 11 (1976) 1278.

[18] A.R. Smith, R.J. McDonald, H. Manini, D.L. Hurley, E.B. Norman, M.C. Vella, R.W. Odom, J. Electrochem. Soc. 143 (1996) 339.

[19] T. Buonassisi, A.A. Istratov, M.D. Pickett, M. Heuer, J.P. Kalejs, G. Hahn, M.A. Marcus, B. Lai, Z. Cai, S.M. Heald, T.F. Ciszek, R.F. Clark, D.W. Cunningham, A.M. Gabor, R. Jonczyk, S. Narayanan, E. Sauar, E.R. Weber, Progr. Photovoltaics: Res. Appl. (2006) in press.

[20] O. Breitenstein, unpublished, 2005.

[21] J.P. Kalejs, B. Bathey, C. Dube, J. Crystal Growth 109 (1991) 174.

[22] H. Gottschalk, Phys. Stat. Sol. B 222 (2000) 353.

[23] T. Buonassisi, A.A. Istratov, M.A. Marcus, M. Heuer, M.D. Pickett, B. Lai, Z. Cai, S.M. Heald, E.R. Weber, Solid State Phenom. 108–109 (2005) 577.